GaN Microdisk with Direct Coupled Waveguide for Unidirectional Whispering Gallery Mode Emission

CHAP HANG TO, WAI YUEN FU, KWAI HEI LI, YUK FAI CHEUNG, AND HOI WAI CHOI*

Department of Electrical and Electronic Engineering, The University of Hong Kong, Pokfulam Road, Hong Kong, China
**Corresponding author: hwchoi@hku.hk*

Received 29 October 2019; revised 12 December 2019; accepted 17 December 2019; posted 20 December 2019 (Doc. ID 381767); published 5 February 2020

Microdisks are excellent whispering-gallery mode optical resonators that can be formed on planar wafers, but their emissions are invariably in-plane isotropic due to their circularities, and thus difficult to be extracted efficiently for practical applications. In this work, a waveguide with a width of 0.16 μm coupled a microdisk with a diameter of 10 μm is fabricated on a 0.77 μm thick GaN thin film containing InGaN/GaN multi-quantum wells. The waveguide is connected directly to the microdisk at the circumference forming a coupling junction, eliminating the need for precision patterning as with evanescent coupling schemes whereby gaps of the order of tens of nanometers between the waveguide and resonator must be maintained. The fabrication was carried out using nanosphere and nanowire lithography. Non-evanescent coupling of whispering-gallery modes (WGMs) to the waveguide from the microdisk is successfully demonstrated.

http://dx.doi.org/10.1364/OL.381767

Since the breakthroughs in material qualities in the late 1980s [1, 2], GaN and its alloys have been under intensive study. Due to its large energy bandgap of 3.4 eV, optical transparency in visible range [3] and high optical gain [4], GaN is one of the best candidates for active photonic applications [5–8]. GaN optical cavities generate coherent light which is essential for photonic application. Among various designs, the microdisk is an attractive system for whispering-gallery mode (WGM) generation due to its high quality factor (Q-factor) and low lasing threshold [9, 10].

On the other hand, effective light extraction from the optical cavities is equally important for practical applications. A microdisk resonator radiates isotropically in-plane due to its circularity. A robust and controllable way for coupling the emission from the microdisk into a waveguide is desired. A common approach is the placement of a waveguide in close proximity to the microdisk's circumference so as to allow evanescent wave coupling [11–13].

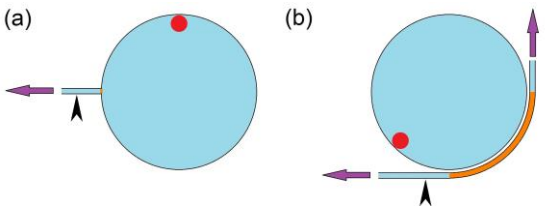

Fig. 1. Configurations of (a) direct coupling and (b) evanescent coupling. The sources are shown as red spots, while the black arrows indicate the monitor positions for measuring the power transmitted into the waveguide.

Efficient evanescent coupling occurs at close proximity (< 100 nm) when there is a phase matching between the light in the waveguide and that in the cavity [12]. The obvious drawback of such an approach is that the gap between the waveguide and the cavity requires fine control to ensure effective coupling, thus the choices of fabrication methods are greatly limited. In this work, we adopt a simple approach to couple light from a microdisk resonator to a waveguide by non-evanescent direct coupling [14–16], which does not rely on delicate control of dimensions and can be achieved effectively by nanosphere and nanowire lithography. Our use of nanospheres [17-19] and nanowires as masking structures enable efficient patterning and fabrication of nanostructures with high throughput and etch selectivity as compared to serial writing processes such as electron beam lithography.

The efficiency of the two coupling methods, schematically shown in Fig. 1, are estimated by 2-D finite-difference time-domain (FDTD) simulations using a commercial software (Lumerical). In both configurations, the simulated microdisks, having diameters of 10 μm with coupled waveguide widths of 160 nm, are all set to be GaN material [20]. The evanescent coupling length is 1/4 of the circumference of the microdisk while the gap width is 50 nm, based on a recent study [13]. The simulations were carried out with a mesh size equal to 1/40 of wavelength for a duration of 40 ps (time step < 8.56×10^{-6} ps). Stretched coordinate perfectly matched layer (PML) was used as the boundary condition of the simulation region. The locations of the single TE polarized electric dipole and the

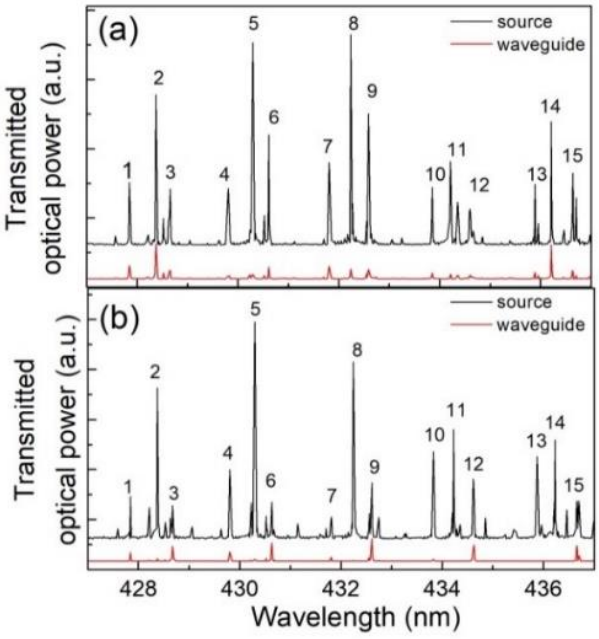

Fig. 2. Simulated power spectra of the sources (black) and transmitted optical signals (red) under the configurations of (a) direct coupling and (b) evanescent coupling.

transmission monitors for recording the optical powers transmitted through the waveguide are indicated as red spots and black arrows respectively in Figs 1(a) and (b), while the coupling regions are highlighted in orange. The resulting optical power spectra from the sources injected into the microdisk-waveguide system (black) and those of transmitted signals (red) are plotted in Fig 2, while the calculated transmission efficiencies are tabulated in Table 1. $TE_{N\rho, N\phi}$ refers to the transverse-electric WGMs where N_ρ is the number of maxima minus one of the electric field energy density in radial direction and N_ϕ is the number of wavelengths of the WGMs within the circumference, respectively. The average output efficiency is 12 % for non-evanescent direct coupling, and 18 % for evanescent coupling. It is noted that the different modes show comparable output efficiencies in the direct coupling scheme, but modes with $N_\rho \neq 0$ are preferably coupled in the evanescent coupling configuration. While the efficiency of direct coupling is lower than that of evanescent coupling, the simplicity of the approach makes it worthy of investigations. The waveguide coupled microdisk structure was formed on a GaN thin film [21], in which the eutectic bonding layer also functions as a mirror to promote optical confinement [22].

Table 1. Output efficiencies η of optical modes (427 - 437 nm)

	Direct			Evanescent		
Peak	dominant mode	λ (nm)	η	dominant mode	λ (nm)	η
1	$TE_{2,160}$	427.84	23 %	$TE_{2,160}$	427.84	21 %
2	$TE_{0,174}$	428.37	23 %	$TE_{0,174}$	428.37	2 %
3	$TE_{1,166}$	428.66	14 %	$TE_{1,166}$	428.67	46 %
4	$TE_{2,159}$	429.81	2 %	$TE_{2,159}$	429.81	14 %
5	$TE_{0,173}$	430.29	10 %	$TE_{0,173}$	430.29	1 %
6	$TE_{1,165}$	430.61	10 %	$TE_{1,165}$	430.63	50 %
7	$TE_{2,158}$	431.81	15 %	$TE_{2,158}$	431.81	16 %
8	$TE_{0,172}$	432.23	5 %	$TE_{0,172}$	432.25	0 %
9	$TE_{1,164}$	432.58	7 %	$TE_{1,164}$	432.61	41 %
10	$TE_{2,157}$	433.85	10 %	$TE_{2,157}$	433.82	2 %
11	$TE_{0,171}$	434.21	5 %	$TE_{0,171}$	434.22	0 %
12	$TE_{1,163}$	434.60	6 %	$TE_{3,151}$	434.61	35 %
13	$TE_{2,156}$	435.89	11 %	$TE_{2,156}$	435.87	0 %
14	$TE_{0,170}$	436.21	28 %	$TE_{0,170}$	436.22	0 %
15	$TE_{1,162}$	436.64	11 %	$TE_{1,162}$	436.65	42 %

Schematic diagrams depicting the fabrication process is shown in Fig. 3. The fabrication began with the deposition of Ni/Au (30 nm/100 nm) by electron beam (e-beam) evaporation on the p-GaN surface of a patterned-sapphire substrate LED wafer with InGaN/GaN multi-quantum wells (MQWs), followed by rapid thermal annealing (RTA) at 450°C in an O_2 ambient. An Au seeding layer of 100 nm was then deposited onto the annealed metal alloy by e-beam evaporation, followed by the electroplating of Cu and Sn for wafer bonding to a Ti/Au (30 nm/100 nm) coated Si wafer. Laser lift-off (LLO) [23] was proceeded by irradiating a collimated, flat-topped laser beam from a 266 nm Nd:YAG laser onto the polished sapphire surface of the bonded structure for detachment of the substrate. The concave patterns exposed after detachment of the patterned substrate were then removed by mechanical

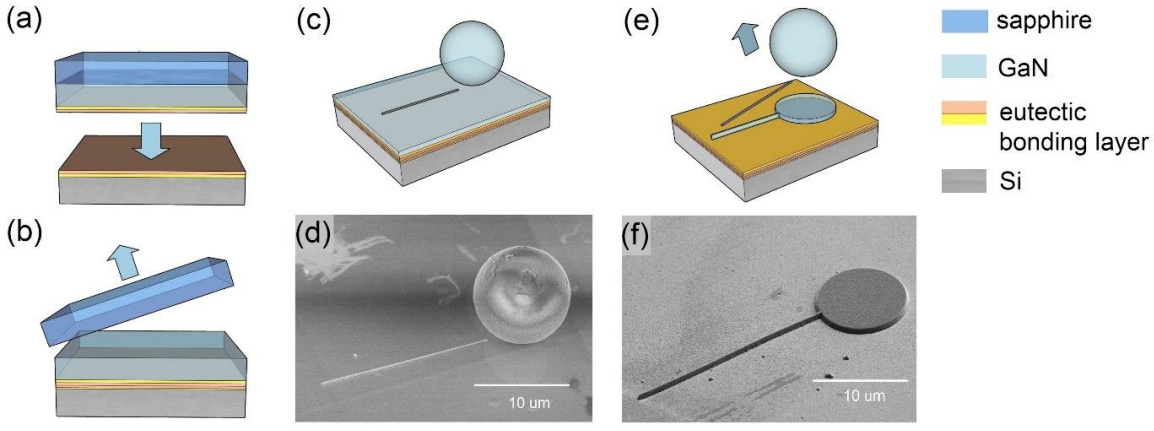

Fig. 3. (a) The GaN wafer was first eutectically bonded to a Si wafer, followed by (b) substrate removal by LLO. After polishing and thinning down of the GaN layer, (c) the nanosphere and the nanowire were then deposited on the GaN thin film surface as hard mask for ICP etching, as shown in (d) the corresponding SEM image. (e) The nanosphere and nanowire were removed after etching, as shown in (f) the corresponding SEM image.

polishing. The polished GaN layer was then thinned down by etching with inductive-coupled-plasma (ICP) etching at a rate of 50 nm/min until the MQWs were almost exposed, resulting in a film with a thickness of ~ 0.77 μm. A suspension of SiO_2 nanospheres with diameters of 10 μm and SiC nanowires with lengths of 20 - 30 μm and diameters of 185 nm (± 53%) were dispensed onto another substrate; suitable nanospheres and nanowires were selected by a steel needle probe with tip radius of 0.5 μm, mounted on a 80 TPI micropositioner . The nanospheres and nanowires were laid down on the GaN thin-film surface manually with positional accuracy of c.a. ± 0.5 μm. The nanospheres and nanowires then served as masks for ICP etching. After pattern transfer, the residual nanospheres and nanowires were removed by hydrofluoric acid (HF) to reveal the waveguide coupled microdisk, as shown in Fig. 3(d). The optical structure was characterized with photoluminescence (PL) spectroscopy at room temperature. The GaN microdisk was excited by a diode-pumped solid-state (DPSS) laser emitting pulses (4 ns, 1 kHz) at 349 nm. The PL signals emitted from the end of the waveguide was collected by a lensed fiber tip with a focal length of c.a. 30 μm and mounted on an x-y-z translation stage, while the other end of the lensed fiber was coupled to a spectrometer (Acton SP2500A) equipped with a cooled charged-coupled device (CCD) (Princeton Instruments PIXIS). An 1800 l/mm grating was used for spectrum dispersion inside the spectrometer.

It was crucial to ensure that the lensed fiber picks up optical signals exclusively from the waveguide exit (c.a. 0.77 μm × 0.16 μm) and exclude those emitted directly from the microdisk. Referring to Fig. 4(a), when low power laser excitation was injected to the microdisk via an auxiliary lensed fiber A, a tiny light spot can be observed at the exit of the waveguide (with microscope objective set at angle θ, approximately 35°, to the horizontal), indicating that a significant PL signal was emitting from the exit of the waveguide. The measuring lensed fiber M was then set at an angle of θ, through which auxiliary low power excitation was injected to visualize the focal spot size of the lensed fiber M, as shown in Fig. 4(b). The elongated focal spot was small and was focused onto the center of the waveguide. Therefore, the lensed fiber M, set at an angle of θ, would not pick up signal from both the microdisk and the waveguide exit simultaneously when the microdisk is pumped. The optimum θ was found to be 30° after several alignments. After fixing the angle of lensed fiber M, auxiliary low power excitation was injected to the microdisk via lensed fiber A, for the purpose of positional alignment. The lensed fiber M was translated across a 9 × 5 grid (step size c.a. 1 μm) to locate the position for receiving optical signal from the exit of the waveguide, as shown in Fig. 4(c). No PL signal could be picked up if the lensed fiber M deviated from the optimum position by c.a. 2 μm. Videos of the alignment process are available as supplementary information.

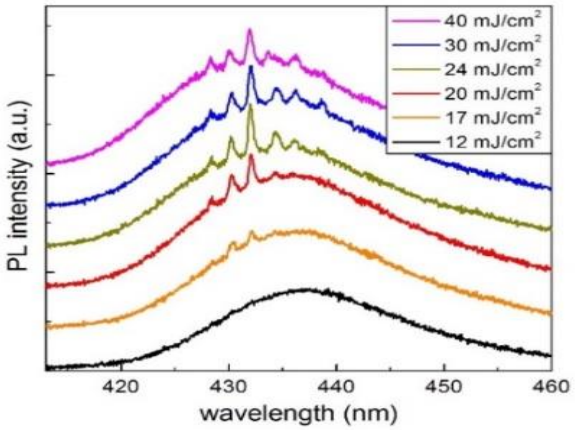

Fig. 5. PL spectra of the transmitted optical signal outputted from the waveguide, taken at different excitation energy densities using a lensed fiber.

The 349 nm laser pulses were focused onto the microdisk at normal incidence, while the PL signal was collected at the exit of the coupling waveguide through the lensed fiber A. The PL spectra collected at different excitation energy densities are plotted in Fig. 5, which have been offset vertically for clarity. At an excitation energy density of 12 mJ/cm², only the broad emission from the MQWs was observed. When the excitation energy density was increased to 17 mJ/cm², two PL peaks emerged at 430 and 432 nm. Additional PL peaks at 428, 434, 436 nm also emerged at peak at increasing excitation energy densities. The Q-factor ($\lambda/\Delta\lambda$) of the 432 nm was in the range of 700 to 800, while the spectral width was c.a. 0.5 nm (FWHM) at various excitation energy densities. The Q-factor is affected by various factors related to the loss of energy from the microdisk including the waveguide coupling scheme as well as the

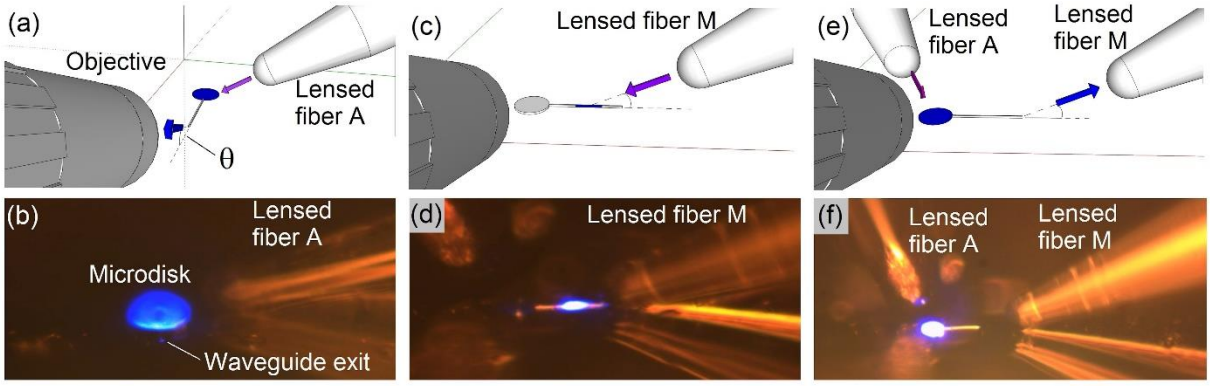

Fig. 4. (a) Schematic diagram and (b) optical microphotograph showing the collection of the PL signal from the exit of the waveguide when the microdisk is under optical excitation. Also refer to **Visualization 1**. (c) Schematic diagram and (d) microphotograph showing the excitation of the middle portion of the waveguide with the focused beam from lensed fiber M. Also refer to **Visualization 2**. (e) Schematic diagram and (f) microphotograph showing the microdisk is subjected to low power optical excitation injected from lensed fiber A, while lensed fiber M receives the excited optical signal at the waveguide exit.

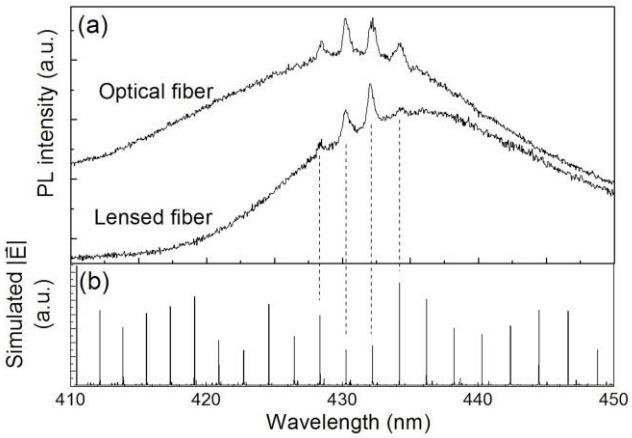

Fig. 6. (a) Spectrum taken directly via an optical fiber and spectrum obtained from exit of waveguide via a lensed fiber. (b) The measured peak wavelengths are consistent with simulations.

sidewall roughness, which can be mitigated by post-ICP chemical treatments [24]. The measured Q-factor is lower than that of the evanescent-coupled GaN microdisk reported in [13], attributed to larger disturbances to the modes due to direct coupling, which is consistent with the observations from previous reports [16, 25-28]. It is also noted that the broad emission from MQWs experienced a blue shift of approximately 5 nm as the excitation energy increased from 12 to 40 mJ/cm^2; this is due to the screening of intrinsic strain-induced piezoelectric fields by the high density carriers at high excitation power, and hence the transition energy of the MQWs increases owing to quantum-confined-stark-effect (QCSE) [29, 30].

The PL signal was also collected directly from the microdisk, not through the coupling waveguide, using an optical fiber placed about 3 mm away at an excitation energy density of 21 mJ/cm^2. This spectrum is compared to that taken at the exit of the waveguide via lensed fiber at an excitation energy density of 20 mJ/cm^2, as shown in Fig. 6. Both spectra showed distinct spectral peaks at the same wavelengths, with free spectral range (FSR) of about 2 nm. For comparison purpose, an unperturbed 10 μm GaN microdisk was simulated. The electric field amplitude spectrum of the WGMs was obtained by field monitors placed within 200 nm of the circumference, while other settings are the same as previous simulations. The peaks in the simulated spectrum are consistent with those in the measured spectra. This demonstrates that the WGMs formed in the microdisk can be effectively coupled to the waveguide through this direct coupling configuration for achieving unidirectional emission.

To summarize, we have successfully fabricated a waveguide (cross section = 0.16 μm × 0.77 μm) coupled microdisk (diameter = 10 μm) structure with nanosphere and nanowire lithography on the GaN thin film platform. The direct connection of a waveguide to the microdisk makes precise positional control during fabrication unnecessary, unlike evanescent coupling schemes where the gap distance between the microdisk and waveguide is critical. Despite the physical connection between the waveguide and the microdisk, WGMs can still be formed and successfully channeled through the waveguide. Thus we demonstrated a robust and economical way to achieve unidirection WGM emission from GaN microdisk.

Fundings This work is jointly supported by General Research Fund (project 17211415) and the NFSC/RGC Joint Research Scheme (N_HKU710/15) of the Research Grant Council of Hong Kong.

Disclosures The authors declare no conflicts of interest.

REFERENCES

1. H. Amano, N. Sawaki, I. Akasaki, and Y. Toyoda, Appl. Phys. Lett. **48**, 353 (1986).
2. H. Amano, M. Kito, K. Hiramatsu, and I. Akasaki, Jpn. J. Appl. Phys. **28**, L2112 (1989).
3. N. Sanford, A. Munkholm, M. Krames, A. Shapiro, I. Levin, A. Davydov, S. SAYAN, L. Wielunski, and T. E. Madey, physica status solidi (c) **2**, 2783 (2005).
4. M. Karaliunas, E. Kuokstis, K. Kazlauskas, S. Jursenas, V. Hoffman, and A. Knauer, (2008).
5. S. Nakamura, M. Senoh, and T. Mukai, Appl. Phys. Lett. **62**, 2390 (1993).
6. S. Rajbhandari, J. J. D. McKendry, J. Herrnsdorf, H. Chun, G. Faulkner, H. Haas, I. M. Watson, D. O'Brien, and M. D. Dawson, Semicond. Sci. Technol. **32**, 023001 (2017).
7. T.-C. Wu, Y.-C. Chi, H.-Y. Wang, C.-T. Tsai, and G.-R. Lin, Sci. Reports **7** (2017).
8. Y. Sun, K. Zhou, Q. Sun, J. Liu, M. Feng, Z. Li, Y. Zhou, L. Zhang, D. Li, S. Zhang, M. Ikeda, S. Liu, and H. Yang, Nat. Photonics **10**, 595 EP (2016).
9. R. A. Mair, K. C. Zeng, J. Y. Lin, H. X. Jiang, B. Zhang, L. Dai, A. Botchkarev, W. Kim, H. Morkoç, and M. A. Khan, Appl. Phys. Lett. **72**, 1530 (1998).
10. G. Zhu, J. Li, J. Li, J. Guo, J. Dai, C. Xu, and Y. Wang, Opt. Lett. **43**, 647 (2018).
11. X.-F. Jiang, C.-L. Zou, L. Wang, Q. Gong, and Y.-F. Xiao, Laser & Photonics Rev. **10**, 40 (2016).
12. M. Cai, O. Painter, and K. Vahala, Phys. Rev. Lett. **85** (2000).
13. F. Tabataba-Vakili, L. Doyennette, C. Brimont, T. Guillet, S. Rennesson, E. Frayssinet, B. Damilano, J.-Y. Duboz, F. Semond, I. Roland, M. El Kurdi, X. Checoury, S. Sauvage, B. Gayral, and P. Boucaud, ACS Photonics **5**, 3643 (2018).
14. Y.-D. Yang, S.-J. Wang, and Y.-Z. Huang, Opt. Express **17**, 23010 (2009).
15. S. Liu, W. Sun, Y. Wang, X. Yu, K. Xu, Y. Huang, S. Xiao, and Q. Song, Optica **5**, 612 (2018).
16. S. Wang, J. Lin, Y. Huang, Y. Yang, K. Che, J. Xiao, Y. Du, and Z. Fan, IEEE Photonics Technol. Lett. **22**, 1349 (2010).
17. R. Chen, H. D. Sun, T. Wang, K. N. Hui, and H. W. Choi, Appl. Phys. Lett. **96**, 241101 (2010).
18. K. H. Li, Z. Ma, and H. W. Choi, Appl. Phys. Lett. **98**, 071106 (2011).
19. Y. Zhang, Z. MA, X. Zhang, T. Wang, and H. Choi, Appl. Phys. Lett. **104**, 221106 (2014).
20. A. S. Barker and M. Ilegems, Phys. Rev. B **7**, 743 (1973).
21. C. Chang, Y. Chuang, and C. Liu, Electrochem. Solid State Lett. **10**, H344 (2007).
22. X. Zhang, C. H. To, and H. W. Choi, Jpn. J. Appl. Phys. **56**, 01AD04 (2016).
23. W. S. Wong, A. B. Wengrow, Y. Cho, A. Salleo, N. J. Quitoriano, N. W. Cheung, and T. Sands, J. Electron. Mater. **28**, 1409 (1999).
24. Y. Yue, X. Yan, W. Li, H. G. Xing, D. Jena, and P. Fay, J. Vac. Sci. & Technol. B **32**, 061201 (2014).
25. Seung June Choi, K. Djordjev, Sang Jun Choi, and P. D. Dapkus, IEEE Photonics Technol. Lett. **15**, 1330 (2003).
26. J. McPhillimy, C. Klitis, S. May, B. Guilhabert, M. D. Dawson, Marc Sorel, and Michael J. Strain, presented at the European Coference On Integrated Optics, Ghent, Belgium, 24-26 April 2019.
27. J. V. Campenhout, P. Rojo-Romeo, P. Regreny, C. Seassal, D. V. Thourhout, S. Verstuyft, L. D. Cioccio, J.-M. Fedeli, C. Lagahe, and R. Baets, Opt. Express **15**, 6744 (2007).
28. D. Liang, M. Fiorentino, T. Okumura, H.-H. Chang, D. T. Spencer, Y.-H. Kuo, A. W. Fang, D. Dai, R. G. Beausoleil, and J. E. Bowers, Opt. Express **17**, 20355 (2009).

29. D. A. B. Miller, D. S. Chemla, T. C. Damen, A. C. Gossard, W. Wiegmann, T. H. Wood, and C. A. Burrus, Phys. Rev. Lett. **53**, 2173 (1984).
30. T. Takeuchi, S. Sota, M. Katsuragawa, M. Komori, H. Takeuchi, H. Amano, and I. Akasaki, Jpn. J. Appl. Phys. **36**, L382 (1997).

FULL REFERENCES

1. H. Amano, N. Sawaki, I. Akasaki, and Y. Toyoda, "Metalorganic vapor phase epitaxial growth of a high quality GN film using an AlN buffer layer," Appl. Phys. Lett. **48**, 353–355 (1986).
2. H. Amano, M. Kito, K. Hiramatsu, and I. Akasaki, "P-type conduction in Mg-doped GaN treated with low-energy electron beam irradiation (LEEBI)," Jpn. J. Appl. Phys. **28**, L2112–L2114 (1989).
3. N. Sanford, A. Munkholm, M. Krames, A. Shapiro, I. Levin, A. Davydov, S. SAYAN, L. Wielunski, and T. E. Madey, "Refractive index and birefringence of InxGa1–xN films grown by MOCVD," physica status solidi (c) **2**, 2783 – 2786 (2005).
4. M. Karaliunas, E. Kuokstis, K. Kazlauskas, S. Jursenas, V. Hoffman, and A. Knauer, "Optical gain dynamics in InGaN/InGaN quantum wells," (2008).
5. S. Nakamura, M. Senoh, and T. Mukai, "High-power InGaN/GaN double-heterostructure violet light emitting diodes," Appl. Phys. Lett. **62**, 2390–2392 (1993).
6. S. Rajbhandari, J. J. D. McKendry, J. Herrnsdorf, H. Chun, G. Faulkner, H. Haas, I. M. Watson, D. O'Brien, and M. D. Dawson, "A review of gallium nitride LEDs for multi-gigabit-per-second visible light data communications," Semicond. Sci. Technol. **32**, 023001 (2017).
7. T.-C. Wu, Y.-C. Chi, H.-Y. Wang, C.-T. Tsai, and G.-R. Lin, "Blue laser diode enables underwater communication at 12.4 Gbps," Sci. Reports **7** (2017).
8. Y. Sun, K. Zhou, Q. Sun, J. Liu, M. Feng, Z. Li, Y. Zhou, L. Zhang, D. Li, S. Zhang, M. Ikeda, S. Liu, and H. Yang, "Room-temperature continuous-wave electrically injected InGaN-based laser directly grown on Si," Nat. Photonics **10**, 595 EP – (2016).
9. R. A. Mair, K. C. Zeng, J. Y. Lin, H. X. Jiang, B. Zhang, L. Dai, A. Botchkarev, W. Kim, H. Morkoç, and M. A. Khan, "Optical modes within III-nitride multiple quantum well microdisk cavities," Appl. Phys. Lett. **72**, 1530 (1998).
10. G. Zhu, J. Li, J. Li, J. Guo, J. Dai, C. Xu, and Y. Wang, "Single-mode ultraviolet whispering gallery mode lasing from a floating GaN microdisk," Opt. Lett. **43**, 647–650 (2018).
11. X.-F. Jiang, C.-L. Zou, L. Wang, Q. Gong, and Y.-F. Xiao, "Whisperinggallery microcavities with unidirectional laser emission," Laser & Photonics Rev. **10**, 40–61 (2016).
12. M. Cai, O. Painter, and K. Vahala, "Observation of critical coupling in a fiber taper to a Silica-microsphere whispering-gallery mode system," Phys. Rev. Lett. **85** (2000).
13. F. Tabataba-Vakili, L. Doyennette, C. Brimont, T. Guillet, S. Rennesson, E. Frayssinet, B. Damilano, J.-Y. Duboz, F. Semond, I. Roland, M. El Kurdi, X. Checoury, S. Sauvage, B. Gayral, and P. Boucaud, "Blue microlasers integrated on a photonic platform on Silicon," ACS Photonics **5**, 3643–3648 (2018).
14. Y.-D. Yang, S.-J. Wang, and Y.-Z. Huang, "Investigation of mode coupling in a microdisk resonator for realizing directional emission," Opt. Express **17**, 23010–23015 (2009).
15. S. Liu, W. Sun, Y. Wang, X. Yu, K. Xu, Y. Huang, S. Xiao, and Q. Song, "End-fire injection of light into high-q Silicon microdisks," Optica **5**, 612–616 (2018).
16. S. Wang, J. Lin, Y. Huang, Y. Yang, K. Che, J. Xiao, Y. Du, and Z. Fan, "AlGaInAs–InP microcylinder lasers connected with an output waveguide," IEEE Photonics Technol. Lett. **22**, 1349–1351 (2010).
17. R. Chen, H. D. Sun, T. Wang, K. N. Hui, and H. W. Choi, "Optically pumped ultraviolet lasing from nitride nanopillars at room temperature," Appl. Phys. Lett. **96**, 241101 (2010).
18. K. H. Li, Z. Ma, and H. W. Choi, "High-q whispering-gallery mode lasing from nanosphere-patterned gan nanoring arrays," Appl. Phys. Lett. **98**, 071106 (2011).
19. Y. Zhang, Z. MA, X. Zhang, T. Wang, and H. Choi, "Optically pumped whispering-gallery mode lasing from 2um gan micro-disks pivoted onsi," Appl. Phys. Lett. **104**, 221106–221106 (2014).
20. A. S. Barker and M. Ilegems, "Infrared lattice vibrations and free electrondispersion in gan," Phys. Rev. B **7**, 743–750 (1973).
21. C. Chang, Y. Chuang, and C. Liu, "Ag au diffusion wafer bonding for thin-gan led fabrication," Electrochem. Solid State Lett. **10**, H344–H346 (2007).
22. X. Zhang, C. H. To, and H. W. Choi, "Optically-free-standing InGaN microdisks with metallic reflectors," Jpn. J. Appl. Phys. **56**, 01AD04 (2016).
23. W. S. Wong, A. B. Wengrow, Y. Cho, A. Salleo, N. J. Quitoriano, N. W. Cheung, and T. Sands, "Integration of gan thin films with dissimilar substrate materials by pd-in metal bonding and laser lift-off," J. Electron. Mater. **28**, 1409–1413 (1999).
24. Y. Yue, X. Yan, W. Li, H. G. Xing, D. Jena, and P. Fay, "Faceted sidewall etching of n-gan on sapphire by photoelectrochemical wet processing," J. Vac. Sci. & Technol. B **32**, 061201 (2014).
25. Seung June Choi, K. Djordjev, Sang Jun Choi, and P. D. Dapkus, "Microdisk lasers vertically coupled to output waveguides," IEEE Photonics Technol. Lett. **15**, 1330–1332 (2003).
26. J. McPhillimy, C. Klitis, S. May, B. Guilhabert, M. D. Dawson, Marc Sorel, and Michael J. Strain, "High accuracy transfer printing of III-V/SOI micro-disk resonators for non-linear applications," presented at the European Coference On Integrated Optics, Ghent, Belgium, 24-26 April 2019.
27. J. V. Campenhout, P. Rojo-Romeo, P. Regreny, C. Seassal, D. V. Thourhout, S. Verstuyft, L. D. Cioccio, J.-M. Fedeli, C. Lagahe, and R. Baets, "Electrically pumped inp-based microdisk lasers integrated with a nanophotonic silicon-on-insulator waveguide circuit," Opt. Express **15**, 6744–6749 (2007).
28. D. Liang, M. Fiorentino, T. Okumura, H.-H. Chang, D. T. Spencer, Y.-H. Kuo, A. W. Fang, D. Dai, R. G. Beausoleil, and J. E. Bowers, "Electrically-pumped compact hybrid silicon microring lasers for optical interconnects," Opt. Express **17**, 20355–20364 (2009).
30. D. A. B. Miller, D. S. Chemla, T. C. Damen, A. C. Gossard, W. Wiegmann, T. H. Wood, and C. A. Burrus, "Band-edge electroabsorption in quantum well structures: The quantum-confined stark effect," Phys. Rev. Lett. **53**, 2173–2176 (1984).
30. T. Takeuchi, S. Sota, M. Katsuragawa, M. Komori, H. Takeuchi, H. Amano, and I. Akasaki, "Quantum-confined stark effect due to piezoelectric fields in GaInN strained quantum wells," Jpn. J. Appl. Phys. **36**, L382–L385 (1997).